Communications in Computational Chemistry
Commun. Comput. Chem., Vol. 7, No. 1, 24–29
doi: 10.4208/cicc.2025.56.01
Regular Article

Effect of Molecule Coverage on Nitric Oxide Reduction Reaction on Cu(111)

Haoran Li, Ying Dai*, Baibiao Huang, Wei Wei*

School of Physics, State Key Laboratory of Crystal Materials, Shandong University,

Jinan 250100, China.

* Corresponding authors: daiy60@sdu.edu.cn (Y. Dai), weiw@sdu.edu.cn (W. Wei)

Received on 05 March 2025; Accepted on 26 April 2025

Abstract: Electrochemical nitrogen oxide reduction reaction (NORR) can simultaneously remove atmospheric pollutant NO and produce the important chemical ammonia (NH_3), which, therefore, has garnered significant attention. However, the effect of molecule coverage on catalyst surface on electrocatalytic activity is less discussed. In combination of atomic *ab initio* thermodynamics and the first-principles calculations, the relationship between the NO coverage and catalytic NORR activity on Cu(111) is unraveled in this work. Results indicate that the adsorption stability and the limiting potential (U_L) of NORR on Cu(111) is closely related to NO coverage. In case of standard conditions (1 atm, 300 K), NO adsorption with a coverage of 1/4 monolayer (ML) is the most stable configuration, though the corresponding U_L (0.34 V) is higher than those of 1/9 (0.29 V) and 1/16 ML (0.29 V) adsorption while significantly lower than that of 1 ML (0.78 V). Therefore, our study provides insights into the role of temperature, pressure and molecule coverage in the electrochemical reactions.

Key words: NORR, Cu(111), molecule coverage, first-principles calculations.

1. Introduction

Nitric oxide (NO) is a major atmospheric pollutant. Excessive emission of NO contributes to environmental issues including acid rain, photochemical smog and global warming, all of which not only cause significant disruptions to human life but also pose substantial threats to public health and survival [1-6]. To address this issue, various denitrification methods have been proposed, with selective catalytic reduction (SCR) being the most widely utilized technology. Through SCR, NO can be converted into harmless nitrogen (N_2) gas and released into the atmosphere [7]. However, SCR presents several challenges including high consumption of expensive reactants and excessive energy requirements, making it economically unfeasible and environmentally unsustainable [8-11].

Ammonia (NH_3) is one of the most important chemicals in industry, with widespread applications in the production of explosives, synthetic fibers, fertilizers and pharmaceuticals. Currently, NH_3 production in industry primarily relies on the Haber–Bosch process, which requires harsh conditions of high temperature and high pressure, accompanied by substantial energy consumption and the release of significant amounts of greenhouse gases [12-15]. In order to overcome these drawbacks, electrochemical N_2 reduction reaction (NRR) has recently garnered intensive interest. NRR occurs under mild conditions and does not generate large amounts of polluting gases, manifesting itself a promising alternative to the Haber–Bosch technology and attracting significant attention [16, 17]. However, NRR faces two significant challenges: 1) low catalytic activity due to the chemical inertness of N_2, and 2) low Faradaic efficiency (FE) because of the competing hydrogen evolution reaction (HER). Therefore, there is an urgent need to explore sustainable and environmentally friendly alternatives for efficient NH_3 production.

It should be emphasized that the cleavage energy of N–O bond is considerably lower than that required to dissociate the ultrastable N≡N triple bond, and thus the N–O bond is more amenable to activation. Therefore, utilizing highly soluble nitrogen oxides, such

as nitrate (NO_3^-), nitrite (NO_2^-) and NO, as alternative nitrogen sources to N_2 presents a promising strategy for the sustainable production of green ammonia [18]. In this context, the concept of directly electrochemically reducing NO to simultaneously remove NO and synthesize NH_3 has been put forward [19-24], which has quickly gained extensive attention as NO exhibits higher chemical reactivity than N_2. In addition, electrocatalytic nitric oxide reduction reaction (NORR) involves a five-electron transfer process for NH_3 synthesis, rendering it energetically more favorable compared to the more complex reduction pathways of nitrite and nitrate [25-27]. Experimental and theoretical studies have reported various electrocatalysts for NORR, such as Pt (111) [28], defective hexagonal boron nitride [29], as well as CoN_4 moiety [30]. In particular, Cu(111) was demonstrated to have relatively high catalytic NORR activity and excellent NH_3 selectivity, by investigating the adsorption free energy of NORR intermediates on different transition metals [19]. It should be emphasized that, for NORR, N–N coupling under high NO concentrations will lead to the formation of byproducts such as N_2O (with a global warming potential 298 times greater than CO_2) and N_2. It was found that, additionally, the generation of single N products (NH_3) on Cu (111) is favored at low NO coverages [31]. It therefore can be concluded that the electrochemical reaction and the catalytic NORR activity on Cu(111) is in close relation with the molecule coverage on catalyst surface. Unraveling this relationship is of importance for optimizing the activity and selectivity and helps further understanding the NORR mechanism. However, a comprehensive study on the effect of NO coverage on NORR is missing.

In this work, based on the atomic *ab initio* thermodynamics in conjunction with first-principles calculations, we find that the NO molecular coverage on Cu(111) affects the catalytic NORR activity and there is a competition between the stability of adsorption structure and the NORR limiting potential (U_L). In the case for high coverage of 1 monolayer (ML), inter-molecular repulsion inhibits NO activation, resulting in a high energy barrier of 0.78 eV for the potential-determining step (PDS). It is of interest to see that the U_L decreases to 0.34, 0.29 and 0.29 V as the NO coverage decreases to 1/4, 1/9 and 1/16 ML, respectively. It should be emphasized that the adsorption structure with a 1/4 ML NO coverage is the most stable one under standard conditions (1 atm, 300 K), though it does not provide the optimum catalytic NORR activity. In this view, therefore, our results provide new insights into the effect of molecular coverage on the catalytic activity in electrochemical reactions.

2. Calculation methods

In this work, the first-principles calculations based on spin-polarized density functional theory (DFT) were performed by using the Vienna *ab initio* simulation package (VASP) [32,33]. In order to describe the core–valence interactions, projector-augmented wave (PAW) [34] method was used with a cutoff energy of 500 eV for the plane wave basis set. In the framework of generalized gradient approximation (GGA), Perdew–Burke–Ernzerhof (PBE) [35-37] scheme was applied for the exchange–correlation functional. The convergence criteria for energy and residual force were set to 10^{-5} eV and 0.01 eV/Å, respectively, and Monkhorst–Pack *k*-point mesh of 3×3×1 was used for structure optimization and total energy calculation. To account for the van der Waals (vdW) interactions between the catalyst and NORR intermediates, DFT–D2 scheme was employed [38]. Cu(111) was simulated by a slab model, and a vacuum layer of 20 Å along the z direction was added to avoid the interactions between periodic images.

In light of the atomic *ab initio* thermodynamics, surface free energy γ can be considered to determine the stability of a surface in contact with a gas phase reservoir, which is defined as

$$\gamma(T,\{p_{\mathrm{NO}}\}) = \frac{1}{A}\left[G^{\mathrm{surf}} - n_{\mathrm{Cu}}\mu_{\mathrm{Cu}}^{\mathrm{bulk}} - n_{\mathrm{NO}}\mu_{\mathrm{NO}}^{\mathrm{gas}}(T,p_{\mathrm{NO}})\right]$$

where G^{surf} is the Gibbs free energy of the solid exposing the surface, A is the surface area, and $\mu_{\mathrm{Cu}}^{\mathrm{bulk}}$ and $\mu_{\mathrm{NO}}^{\mathrm{gas}}$ are the chemical potentials of Cu in bulk phase and gaseous NO. In particular, the chemical potential of NO molecular in gas phase as a function of pressure p and temperature T can be written as

$$\mu_{\mathrm{NO}}^{\mathrm{gas}}(T,p_{\mathrm{NO}}) = E_{\mathrm{NO}}(0\mathrm{K}) + \mu_{\mathrm{NO}}^{'}\left(T,p_{\mathrm{NO}}^{0}\right) + k_{\mathrm{B}}T\lg\left(\frac{p}{p^{0}}\right)$$

where $E_{\mathrm{NO}}(0\mathrm{K})$ is the tot energy from DFT calculations, k_{B} is the Boltzmann constant, and $\mu_{\mathrm{NO}}^{'}\left(T,p_{\mathrm{NO}}^{0}\right)$ can be attained from JANAF thermochemical table [39].

To evaluate the stability of NO adsorption on Cu(111) surface, Gibbs free energy of adsorption ΔG^{ads} was calculated, which can be defined as [40,41]

$$\begin{aligned}
&\Delta G^{\mathrm{ads}}(\Delta\mu_{\mathrm{NO}}) \\
&= \gamma_{\mathrm{Cu}(111)} - \gamma_{\mathrm{NO/Cu}(111)} \\
&= -\frac{1}{A}\left[G_{NO/Cu(111)}^{\mathrm{surf}} - G_{Cu(111)}^{\mathrm{surf}}\right. \\
&\left. - \Delta n_{\mathrm{Cu}}\mu_{\mathrm{Cu}}^{\mathrm{bulk}} \quad - n_{\mathrm{NO}}(E_{\mathrm{NO}} + \Delta\mu_{\mathrm{NO}})\right] \\
&\approx -\frac{1}{A}\tilde{E}_{NO/Cu(111)}^{\mathrm{bind}} + \frac{n_{\mathrm{NO}}}{A}\Delta\mu_{\mathrm{NO}}
\end{aligned}$$

where $G_{\mathrm{NO/Cu}(111)}^{\mathrm{surf}}$ and $G_{\mathrm{Cu}(111)}^{\mathrm{surf}}$ are the Gibbs free energies of the Cu(111) with n_{NO} adsorbed NO molecules and the clean Cu(111), respectively. In particular, the chemical potential of NO is constituted by the total energy part and the temperature- and pressure-dependent term, that is,

$$\mu_{\mathrm{NO}} = E_{\mathrm{NO}}(0\mathrm{K}) + \Delta\mu_{\mathrm{NO}}(T,p)$$

It has been confirmed that the difference between the Gibbs free energies of the clean and adsorbate covered surfaces can be attained from the DFT results [42,43].

In accordance to the computational hydrogen electrode (CHE) model proposed by Nørskov *et al.*, [44] the Gibbs free energy change for each NORR step can be determined by

$$\Delta G = \Delta E + \Delta E_{\mathrm{ZPE}} - T\Delta S$$

where ΔE represents the reaction energy of each elementary step, ΔE_{ZPE} stands for the zero-point energy change and ΔS symbolizes the entropy change, and T is set to the room temperature (298.15 K). In an O-distal reaction pathway, the NORR proceeds continuously following

$$NO(g) + * \rightarrow * NO$$

$$* NO + H^+ + e^- \rightarrow * NOH$$

$$* NOH + H^+ + e^- \rightarrow * N + H_2O(g)$$

$$* N + H^+ + e^- \rightarrow * NH$$

$$* NH + H^+ + e^- \rightarrow * NH_2$$

$$* NH_2 + H^+ + e^- \rightarrow * NH_3$$

3. Results and discussion

It has already been known that the adsorption and activation of NO is the first while the most crucial step in the NORR process, which is essential for the entire electrocatalytic reaction. In other words, sufficient NO adsorption strength is required and efficient NO activation facilitates the initial protonation step thermodynamically easier. It has been demonstrated that the molecule on Cu(111) tends to be adsorbed at the CuCuCu hollow site among the possible NO adsorption sites (Cu site, Cu–Cu bridge site and CuCuCu hollow site) in a N-end configuration [45]. On Cu(111), furthermore, the NORR pathway is confirmed to follow the O-distal pattern, as illustrated in Figure 1a. In this reaction pathway, $H^+ + e^-$ first attacks the distal O atom of NO, resulting in the formation of a H_2O molecule. Subsequently, the coupled $H^+ + e^-$ continues to attack the remaining N atom, eventually producing NH_3 molecule, which then detaches from the catalyst surface. It is important to mention that the generation of byproducts other than NH_3 is a significant challenge for the NORR process. In particular, NO adsorption of high coverage gives rise to a large possibility for the formation of N–N coupled compounds, which ultimately synthesizes byproducts such as N_2 and N_2O [46]. In this view, the FE of NH_3 production is seriously reduced. In Figure 1b, possible pathways for the electrochemical formation of N–N coupled byproducts (N_2O and N_2) on Cu(111) surface are schematically illustrated. In case for high-coverage adsorptions, O-end adsorption can be excluded because the binding is too weak. In the first place, alternatively, two NO molecules co-adsorb on the surface in N-end configuration and NO–NO dimer forms, and then a H_2O molecule is released after two consecutive protonation steps. The resulting deleterious $*N_2O$ may either desorb directly from the surface or be further hydrogenated to produce N_2 and H_2O. In addition, the remaining $*N_2O$ may transition to a NO-side adsorption configuration, leading to the desorption of a N_2 molecule, and the residual *O atom subsequently undergoes hydrogenation and forms H_2O.

To simulate different NO coverages, Cu(111) supercells of 1×1 (with a surface lattice parameter of approximately 2.58 Å), 2×2, 3×3 and 4×4 are considered. In the case of 1×1 Cu(111), one NO molecule adsorption on the surface corresponds to a coverage of 1 ML, and thus 1/4, 1/9 and 1/16 ML for the 2×2, 3×3 and 4×4 counterparts, respectively. In Figure 2a, optimized adsorption configurations of NO on Cu(111) are shown. It can be found that, at different coverages, the NO molecule remains the N-end adsorption configuration over the CuCuCu hollow site. It should be pointed out that, however, the NO bond lengths differ as NO coverage decreases, which can be explained by the reduced inter-molecule repulsive interactions when the coverage decreases. In particular, the N-O bond length turns out to be 1.197, 1.220, 1.222 and 1.227 Å for 1, 1/4, 1/9 and 1/16 ML, respectively. In comparison to the NO bond length of 1.169 Å in gas phase, the stretched bond length on Cu(111) indicates that the molecule is sufficiently activat-

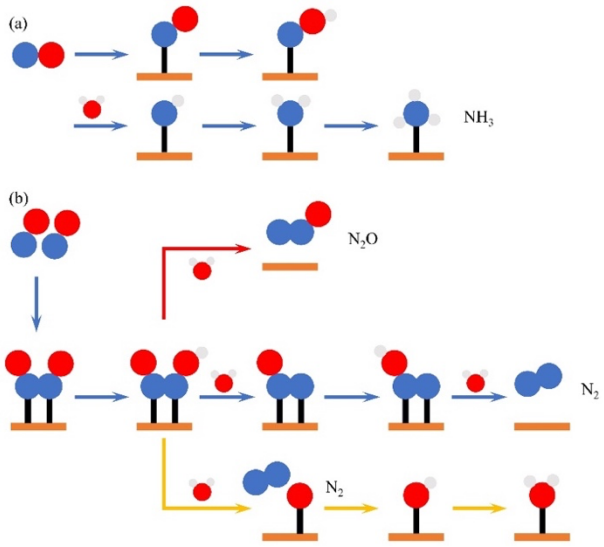

Figure 1. (a) Reaction pathway of electrocatalytic NORR toward NH_3 formation in O-distal pattern. (b) Possible reaction pathways for synthesizing N–N coupled products (N_2 and N_2O) with high NO adsorption coverage. White, blue and red spheres indicate H, N and O atoms, respectively.

ed, which is crucial for the subsequent NORR. In accordance the Sabatier principle, moderate NO adsorption is in favor of NORR; either too strong or too weak adsorption strength can degrade the catalytic activity (insufficient activation or arduous desorption). It appears that low coverage signifies high NO activation and thus high catalytic NORR activity, while adsorption of low NO converge may not stable under standard conditions. In this view, the effect of NO coverage on NORR should be further discussed, aiming at providing an insight into the correlation between structure stability and catalytic activity.

In order to evaluate the stability of NO adsorption of different coverages on Cu(111), adsorption Gibbs free energy (ΔG^{ads}) of these configurations are calculated and compared with the surface free energy of clean Cu(111). In accordance to the definition, $\Delta G^{ads} > 0$ implies that the structure is stable upon adsorption, while a negative value means that the molecule cannot be adsorbed on the catalyst surface. In Figure 2b, Gibbs free energy diagram of NO adsorption on Cu(111) is presented for cases with different molecule coverages, with the gas pressure fixed at one standard atmosphere ($p_{NO} = 1$ atm). It is evident that the adsorption Gibbs free energy of NO exhibits a linear dependence on temperature (or NO chemical potential) and, naturally, the adsorption on Cu(111) turns out to be unstable as temperature increases. In respect to the 1 ML NO coverage, inter-molecular interactions lead to instability of the adsorption structure and the Gibbs free energy for NO adsorption is more sensitive to temperature compared to those of low coverages. It can be observed that the stability for NO adsorption with a coverage of 1 ML decreases rapidly as temperature increases, and the molecule will desorb from the surface when the temperature achieves 340 K. It should be noted that 1 ML NO adsorption will become the most stable configuration among all the coverages of consideration only

when the temperature is lower than 247 K (corresponding to a chemical potential of $\Delta\mu_{NO}$ = –0.45 eV). It therefore is an indication that extremely high coverage of NO adsorption (1 ML) is not favored on Cu(111), which is consistent with experimental observations [31]. It is of interest that, alternatively, NO adsorption with a molecule coverage of 1/4 ML is the most stable pattern over a large temperature range (from 247 to 450 K). In case the temperature is elevated, naturally, NO adsorption of low coverages turns out to be stable; for instance, 1/9 ML coverage is the most favored one as the temperature is higher than 450 K. It can be concluded that there should be an optimum match between NO adsorption coverage and catalytic NORR activity upon Cu(111) at standard conditions.

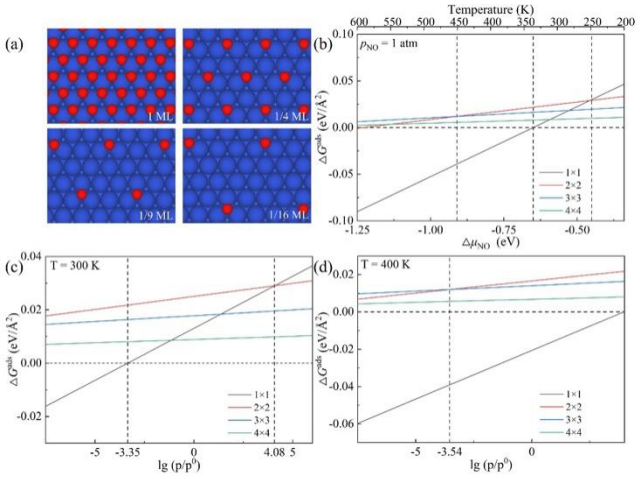

Figure 2. (a) Top views of NO adsorption on Cu(111) with different coverages. Blue and red balls represent Cu and O atoms, respectively. (b) Gibbs free energy ΔG^{ads} as a function of $\Delta\mu_{NO}$ for NO adsorption on Cu(111) under standard atmospheric pressure. Gibbs free energy ΔG^{ads} as a function of lg(p/p^0) for NO adsorption on Cu(111) at (c) 300 K and (d) 500 K. In (b)–(d), curves in different color stands for results based on different Cu(111) supercells, *i.e.*, different NO coverages.

In addition to temperature, the influence of gas pressure on NO adsorption Gibbs free energy should also be considered. In Figure 2c, when NO pressure (lg(p/p^0)) changes, Gibbs free energies for NO adsorption of different coverages on Cu(111) are compared at room temperature (*i.e.*, 300 K). It can be found that high molecule coverage (1 ML) is preferred only when lg(p/p^0) > 4.08, and NO desorbs from the catalyst surface as lg(p/p^0) < –3.35. In consistent with the above discussion, 1/4 coverage dominates the NO adsorption on Cu(111). In Figure 2d, Gibbs free energy of NO adsorption as a function of gas pressure is also presented at higher temperature, *i.e.*, 400 K, to explore the variation trend of the stability of the NO/Cu(111) structures. It can be seen that the stability for NO adsorption on Cu(111) deteriorates, as temperature increases. In this case (at 400 K), coverage of 1/4 ML remains primary as lg(p/p^0) > –3.54, and the surface prefers low NO coverage (1/9 ML) when lg(p/p^0) < –3.54.

In Figure 3a, free energy diagrams for the NORR process on Cu(111) under different NO coverages are presented, and the optimized intermediate (*i.e.*, *NO, *NOH, *N, *NH, *NH_2 and *NH_3) adsorption configurations are provided in Figure 3b. It is of interest to see that the PDS for the NORR on Cu(111) with different molecule coverages remains the first hydrogenation step *NO + H^+ + e^- → *NOH, where a thermodynamic energy barrier is encountered. In subsequent steps, the *NOH combines with H^+ + e^- to form a free H_2O molecule, and the remaining *N will continue to be reduced spontaneously to *NH, *NH_2 and *NH_3. It obviously shows that the energy barrier encountered during the reaction decreases with varying NO coverage, though the PDS remains the first electrochemical reaction step. In particular, the U_L for the NORR on 1×1 Cu(111) (1 ML NO coverage) is as large as 0.78 V, signifying an inferior catalytic NORR activity. In case the NO coverage decreases to 1/4, 1/9 and 1/16 ML, the U_L for NORR on Cu(111) decreases gradually to 0.34, 0.29 and 0.29 V, respectively. In accordance to the Bader charge analysis, the charge transferred from the substrate to *NO is quantified as 0.39, 0.51, 0.55 and 0.57 e^- for 1, 1/4, 1/9 and 1/16 ML adsorption, respectively, confirming the activation effect of the Cu(111) toward NO molecule. It is consistent with the gradual increase in the N–O bond length as the NO adsorption coverage decreases.

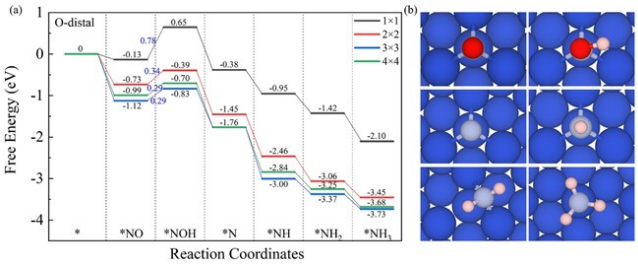

Figure 3. (a) Free energy diagram for NORR on Cu(111) supercells of consideration (corresponding to different NO coverages). Numbers in blue are the U_L. (b) Stable adsorption configurations of the key intermediates for NORR on Cu(111). Blue, gray, red and pink spheres represent Cu, N, O and H atoms, respectively.

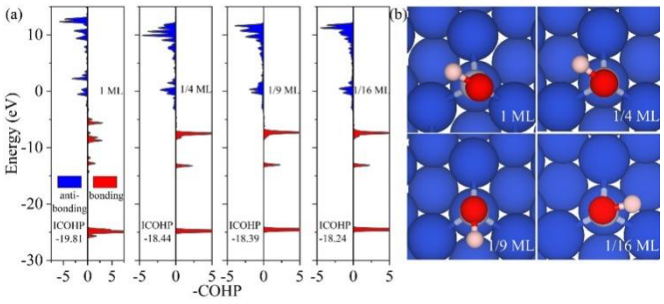

Figure 4. (a) Crystal orbital Hamilton population (COHP) on NO after adsorption (corresponding to different NO coverages), and the Fermi level is set to zero. (b) Stable adsorption structures of key intermediate *NOH at different NO coverages.

In Figure 4a, crystal orbital Hamilton population (COHP) for adsorbed NO is presented, where positive and negative values correspond to bonding and anti-bonding states, respectively. In particular, integrated COHP (ICOHP) can be employed to effectively characterize the bonding strength, with more negative ICOHP indicating stronger interaction. It can be seen that the ICOHP varies as –19.81 (1 ML), –18.44 (1/4 ML), –18.39 (1/9 ML) and –18.24 (1/16 ML), consistent with the NO bond length under different molecule coverages. In Figure 4b, the adsorption structures of intermediate *NOH at different NO coverages are illustrated. It is evident that no significant structure difference can be found after the

first hydrogenation of NO, while the corresponding U_L is different. It therefore highlights the effect of molecule coverage on the catalytic NORR activity. In consideration of both the adsorption stability and activity, NO coverage of 1/4 ML is more preferred for electrocatalytic NORR on Cu(111) (with U_L being 0.34 V). It should be emphasized that tuning the coordination microenvironment and the local electronic structure by, for instance, *p*-block atom doping on surface can probably eliminate the thermodynamic energy barrier in the first hydrogenation step of the NORR on Cu(111). In light of regulating the surface chemical environment and local physical properties, for instance, the incorporation of Si atoms into Cu(111) can successfully eliminate the thermodynamic energy barrier and make the NORR on Cu(111) spontaneous [47].

4. Conclusion

In summary, we demonstrated that the NO molecular coverage is directly related to the catalytic NORR activity on Cu(111) by the first-principles calculations in combination with atomic *ab initio* thermodynamics. In particular, NO activation and the NORR U_L differ with varying molecule coverage, which can be attributed to the reduced inter-molecular repulsive interactions as the coverage decreases. It can be found that 1/4 ML NO adsorption is the most stable configuration under standard conditions (1 atm, 300 K), with the NORR U_L being 0.34 V. In comparison to the metastable 1/9 (U_L = 0.29 V) and 1/16 ML (U_L = 0.29 V) NO adsorption, 1/4 ML NO adsorption obviously does not correspond to the optimum catalytic NORR activity. In this view, our work conclusively confirms the effect of NO molecular coverage on the NORR on Cu(111), providing new insights into the relationship between temperature, pressure and electrocatalytic activity and highlighting the crucial role of molecular coverage in catalyst performance.

Acknowledgements

This work is supported by National Natural Science Foundation of China (52272223).

References

[1] Ren, Z., Zhang, H., Wang, S., Huang, B., Dai, Y., Wei, W. Nitric oxide reduction reaction for efficient ammonia synthesis on topological nodal-line semimetal Cu2Si monolayer. *J. Mater. Chem. A*, **10** (2022), 8568–8577.

[2] Qian, H., Xu, S., Cao, J., Ren, F., Wei, W., Meng, J., Wu, L. Air pollution reduction and climate co-benefits in China's industries. *Nat. Sustain.*, **4** (2021), 417–425.

[3] Li, K., Jacob, D. J., Liao, H., Zhu, J., Shah, V. S., Shen, L., Bates, K. H., Zhang, Q., Zhai, S. A two-pollutant strategy for improving ozone and particulate air quality in China. *Nat. Geosci.*, **12** (2019), 906–910.

[4] Meng, D., Zhan, W., Guo, Y., Guo, Y., Wang, L., Lu, G. A highly effective catalyst of Sm-MnOx for the NH3-SCR of NOx at low temperature: promotional role of Sm and its catalytic performance. *ACS Catal.*, **5** (2015), 5973–5983.

[5] Wu, Q., Wang, H., Shen, S., Huang, B., Dai, Y., Ma, Y. Efficient nitric oxide reduction to ammonia on a metal-free electrocatalyst. *J. Mater. Chem. A*, **9** (2021), 5434–5441.

[6] Lee, T., Bai, H. Low temperature selective catalytic reduction of NOx with NH3 over Mn-based catalyst: a review. *Aims Environ. Sci.*, **3** (2016), 261–289.

[7] Koebel, M., Madia, G., Elsener, M. Selective catalytic reduction of NO and NO2 at low temperatures. *Catal. Today*, **73** (2002), 239–247.

[8] Zhang, R., Liu, N., Lei, Z., Chen, B. Selective transformation of various nitrogen-containing exhaust gases toward N2 over zeolite catalysts. *Chem. Rev.*, **116** (2016), 3658–3721.

[9] Burch, R., Breen, J. P., Meunier, F. C. A review of the selective reduction of NOx with hydrocarbons under lean-burn conditions with non-zeolitic oxide and platinum group metal catalysts. *Appl. Catal. B*, **39** (2002), 283–303.

[10] Forzatti, P. Present status and perspectives in De-NOx SCR catalysis. *Appl. Catal. A Gen.*, **222** (2001), 221–236.

[11] Kim, C. H., Qi, G., Dahlberg, K., Li, W. Strontium-doped perovskites rival platinum catalysts for treating NOx in simulated diesel exhaust. *Science*, **327** (2010), 1624–1627.

[12] Lv, X., Wei, W., Huang, B., Dai, Y., Frauenheim, T. High-throughput screening of synergistic transition metal dual-atom catalysts for efficient nitrogen fixation. *Nano Lett.*, **21** (2021), 1871–1878.

[13] Ma, Z., Xiao, C., Cui, Z., Du, W., Li, Q., Sa, R., Sun, C. Defective Fe3GeTe2 monolayer as a promising electrocatalyst for spontaneous nitrogen reduction reaction. *J. Mater. Chem. A*, **9** (2021), 6945–6954.

[14] Chen, Z., Yan, J.-M., Jiang, Q. Single or double: which is the altar of atomic catalysts for nitrogen reduction reaction? *Small Methods*, **3** (2019), 1800291.

[15] Liu, Y., Deng, P., Wu, R., Zhang, X., Sun, C., Li, H. Oxygen vacancies for promoting the electrochemical nitrogen reduction reaction. *J. Mater. Chem. A*, **9** (2021), 6694–6709.

[16] Jasin Arachchige, L., Xu, Y., Dai, Z., Zhang, X., Wang, F., Sun, C. Double transition metal atoms anchored on graphdiyne as promising catalyst for electrochemical nitrogen reduction reaction. *J. Mater. Sci. Technol.*, **77** (2021), 244–251.

[17] Li, L., Wang, X., Guo, H., Yao, G., Yu, H., Tian, Z., Li, B., Chen, L. Theoretical screening of single transition metal atoms embedded in MXene defects as superior electrocatalyst of nitrogen reduction reaction. *Small Methods*, **3** (2019), 1900337.

[18] Zheng, X., Yan, Y., Li, X., Liu, Y., Yao, Y. Theoretical insights into dissociative–associative mechanism for enhanced electrochemical nitrate reduction to ammonia. *J. Hazard. Mater.*, **446** (2023), 130679.

[19] Long, J., Chen, S., Zhang, Y., Guo, C., Fu, X., Deng, D., Xiao, J. Direct electrochemical ammonia synthesis from nitric oxide. *Angew. Chem. Int. Ed.*, **59** (2020), 9711–9718.

[20] Shi, J., Wang, C., Yang, R., Chen, F., Meng, N., Yu, Y., Zhang, B. Promoting nitric oxide electroreduction to ammonia over electron-rich Cu modulated by Ru doping. *Sci. China Chem.*, **64** (2021), 1493–1497.

[21] Long, J., Guo, C., Fu, X., Jing, H., Qin, G., Li, H., Xiao, J. Unveiling potential dependence in NO electroreduction to ammonia. *J. Phys. Chem. Lett.*, **12** (2021), 6988–6995.

[22] Jiao, D., Liu, Y., Cai, Q., Zhao, J. Coordination tunes the activity and selectivity of the nitrogen reduction reaction on single-atom iron catalysts: a computational study. *J. Mater. Chem. A*, **9** (2021), 1240–1251.

[23] Choi, J., Du, H., Nguyen, C. K., Suryanto, B. H. R., Simonov, A. N., MacFarlane, D. R. Electroreduction of nitrates, nitrites, and gaseous nitrogen oxides: a potential source of ammonia in dinitrogen reduction studies. *ACS Energy Lett.*, **5** (2020), 2095–2097.

[24] Peng, X., Mi, Y., Bao, H., Liu, Y., Qi, D., Qiu, Y., Zhou, L., Zhao, S., Sun, J., Tang, X., Luo, J., Liu, X. Ambient electrosynthesis of ammonia with efficient denitration. *Nano Energy*, **78** (2020), 105321.

[25] Su, Q., Zhang, G., Zhao, T., Chu, K., Cai, Q., Zhao, J. Construction of frustrated Lewis pairs in ZnO surface for boosting electrocatalytic NO reduction to NH3: theoretical prediction and experimental validation. *Appl. Catal. B*, **357** (2024), 124251.

[26] Wang, S., Huang, B., Dai, Y., Wei, W. Electrochemical ammonia synthesis at p-block active sites using various nitrogen sources: theoretical insights. *J. Phys. Chem. Lett.*, **16** (2025), 889–903.

[27] Sun, Y., Huang, B., Dai, Y., Wei, W. Improving nitric oxide reduction reaction activity of TMN4–C model catalysts by axial atom coordination. *J. Phys. Chem. Lett.*, **16** (2025), 9–16.

[28] Clayborne, A., Chun, H.-J., Rankin, R. B., Greeley, J. Elucidation of pathways for NO electroreduction on Pt(111) from first principles. *Angew. Chem. Int. Ed.*, **54** (2015), 8255–8258.

[29] Sun, P., Wang, W., Zhao, X., Dang, J. Defective H-BN sheet embedded atomic metals as highly active and selective electrocatalysts for NH3 fabrication via NO reduction. *Phys. Chem. Chem. Phys.*, **22** (2020), 22627–22634.

[30] Wang, Z., Zhao, J., Wang, J., Cabrera, C. R., Chen, Z. A Co-N4 moiety embedded into graphene as an efficient single-atom-catalyst for NO electrochemical reduction: a computational study. *J. Mater. Chem. A*, **6** (2018), 7547–7556.

[31] Ko, B. H., Hasa, B., Shin, H., Zhao, Y., Jiao, F. Electrochemical reduction of gaseous nitrogen oxides on transition metals at ambient conditions. *J. Am. Chem. Soc.*, **144** (2022), 1258–1266.

[32] Kresse, G., Furthmüller, J. Efficient iterative schemes for ab initio total-energy calculations using a plane-wave basis set. *Phys. Rev. B*, **54** (1996), 11169–11186.

[33] Kresse, G., Joubert, D. From ultrasoft pseudopotentials to the projector augmented wave method. *Phys. Rev. B*, **59** (1999), 1758–1775.

[34] Perdew, J. P., Wang, Y. Accurate and simple analytic representation of the electron-gas correlation energy. *Phys. Rev. B*, **45** (1992), 13244–13249.

[35] Becke, A. D. Density-functional exchange-energy approximation with correct asymptotic behavior. *Phys. Rev. A*, **38** (1988), 3098.

[36] Perdew, J. P., Burke, K., Ernzerhof, M. Generalized gradient approximation made simple. *Phys. Rev. Lett.*, **78** (1996), 1396.

[37] Lee, C., Yang, W., Parr, R. G. Development of the Colle-Salvetti correlation-energy formula into a functional of the electron density. *Phys. Rev. B*, **37** (1988), 785.

[38] Liechtenstein, A. I., Anisimov, V. I., Zaanen, J. Density-functional theory and strong interactions: orbital ordering in Mott-Hubbard insulators. *Phys. Rev. B*, **52** (1995), R5467–R5470.

[39] Huang, Y., Wang, G. Water–gas shift reaction over CuxO/Cu(111) (x < 2) from a DFT-MKM-kMC study. *ACS Catal.*, **15** (2025), 4239–4250.

[40] Li, W., Stampfl, C., Scheffler, M. Why is a noble metal catalytically active? The role of the O-Ag interaction in the function of silver as an oxidation catalyst. *Phys. Rev. Lett.*, **90** (2003), 256102.

[41] Reuter, K., Scheffler, M. Oxide formation at the surface of late 4d transition metals: insights from first-principles atomistic thermodynamics. *Appl. Phys. A: Mater. Sci. Process.*, **78** (2004), 793.

[42] Reuter, K., Scheffler, M. Composition, structure, and stability of RuO2(110) as a function of oxygen pressure. *Phys. Rev. B*, **65** (2001), 035406.

[43] Reuter, K., Scheffler, M. Composition and structure of the RuO2(110) surface in an O2 and CO environment: implications for the catalytic formation of CO2. *Phys. Rev. B*, **68** (2003), 045407.

[44] Nørskov, J. K., Rossmeisl, J., Logadottir, A., Lindqvist, L., Kitchin, J. R., Bligaard, T., Jónsson, H. Origin of the overpotential for oxygen reduction at a fuel-cell cathode. *J. Phys. Chem. B*, **108** (2004), 17886–17892.

[45] Wan, H., Bagger, A., Rossmeisl, J. Electrochemical nitric oxide reduction on metal surfaces. *Angew. Chem. Int. Ed.*, **60** (2021), 21966–21972.

[46] Ko, B. K., Hasa, B., Shin, H., Zhao, Y., Jiao, F. Electrochemical Reduction of Gaseous Nitrogen Oxides on Transition Metals at Ambient Conditions. *J. Am. Chem. Soc.* **144**(2022), 1258–1266.

[47] Zhang, B., Dai, Y., Huang, B., Qian, Z., Ahuja, R., Wei, W. Improving nitric oxide reduction reaction through surface doping on superstructures. *Nano Energy*, **123** (2024), 109396.